Hybrid Imaging: Local Staging of Head and Neck Cancer

Martin W. Huellner and Tetsuro Sekine

Introduction

This chapter discusses the local staging of mucosal and extramucosal epithelial malignant disease of the head and neck, with the exception of mucosal melanoma and thyroid malignancies.

The head and neck is the only compartment of the body that is widely accessible to radiological imaging, clinical examination, and noninvasive endoscopy at the same time. The accuracy of each examination method, however, is different depending on the location of the disease. While superficial mucosal spread of cancer is best addressed with endoscopy, some anatomical subsites, especially parts of the hypopharynx, represent blind spots to the clinician. Cancer arising there might go undetected both with endoscopy and clinical examination, and clinicians have to rely on radiological imaging. Assessing the tumor extension in depth is another domain of cross-sectional imaging, although palpation might be more accurate in certain instances, e.g., in determining the infiltration of the prevertebral fascia or in addressing superficial invasion of cortical bone by cancer.

Currently, head and neck cancer is still among the top ten of malignant diseases in developed parts of the world [1]. Reliable statistics on the overall survival of head and neck cancer patients were established starting in the 1970s, and since then a steady increase in survival has been observed (Fig. 1) [1]. This is believed to be due to several factors. First, advanced cancer stages benefit from a continuous improvement in chemotherapy regimens and radiation therapy, including the advent of intensity-modulated radiation therapy (IMRT) [2]. Second, there was an increase in human papillomavirus (HPV)-related cancers in the oral cavity and oropharynx. These cancers tend to occur in a younger population, and their cure is comparably facile. Third, the technical progress of cross-sectional imaging modalities led to an increase in the staging accuracy of tumors. And this is where diagnostic radiologists contribute to patient care.

While computed tomography (CT) and magnetic resonance (MR) imaging are mainstays of local T and N staging, ^{18}F-fluoro-2-deoxy-D-glucose (FDG) positron emission tomography (PET) raised the bars in the detection of small nodal metastases, distant metastases, and second primary tumors. False-positive results in PET are typically due to inflammatory changes, while false-negatives may be encountered in organs with a high physiologic FDG activity, such as

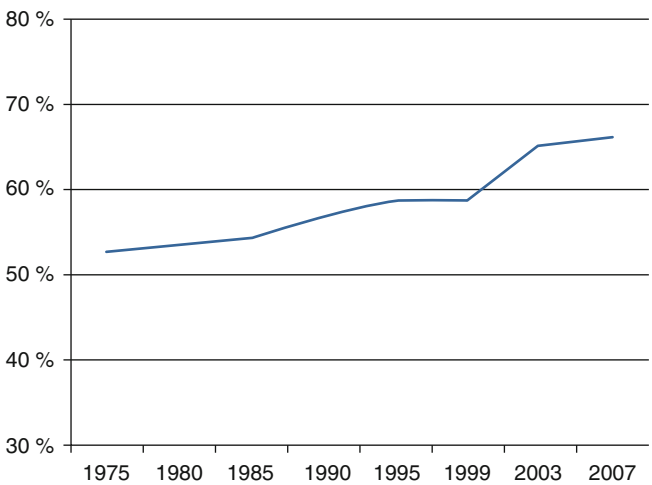

Fig. 1 Five-year relative survival rates in head and neck cancer (Adapted from Pulte et al. [1])

M.W. Huellner (✉)
Division of Nuclear Medicine, Department of Medical Radiology, University Hospital Zurich/University of Zurich, Rämistrasse 100, Zurich 8091, Switzerland

Division of Neuroradiology, Department of Medical Radiology, University Hospital Zurich/University of Zurich, Frauenklinikstrasse 10, Zurich 8091, Switzerland
e-mail: martin.huellner@usz.ch

T. Sekine
Division of Nuclear Medicine, Department of Medical Radiology, University Hospital Zurich/University of Zurich, Rämistrasse 100, Zurich 8091, Switzerland

Department of Radiology, Nippon Medical School, 1-1-5 Sendagi, Bunkyo-ku, Tokyo 113-8603, Japan
e-mail: tetsuro.sekine@usz.ch

J. Hodler et al. (eds.), *Diseases of the Brain, Head and Neck, Spine 2016–2019: Diagnostic Imaging*, DOI 10.1007/978-3-319-30081-8_29

the brain and the liver. Integrated reading of hybrid examinations, either PET/CT or PET/MR, will help classify questionable lesions. Notably, one important pitfall for PET and CT as well as MR exists in the head and neck area: Lymphoepithelial tissue, e.g., in the base of the tongue, takes up both contrast medium and FDG, and indwelling malignant disease might be unnoticed.

Hybrid Imaging of Head and Neck Tumors

The use of FDG-PET in the local staging of head and neck tumors is of limited value. PET activity does not exactly demonstrate the size and extension of a tumor. In larger tumors with high FDG avidity, PET imaging suffers from spillover artifact to surrounding tissues. Smaller tumors (Tis and T1), superficially spreading tumors, or those with low FDG avidity may be missed completely by PET. Therefore, the location and size of a tumor and the depth of invasion need to be accurately identified on contrast-enhanced morphological imaging, using preferably MR, or CT. Small but FDG-avid tumor may hide in regions with high physiologic FDG activity, such as lymphoepithelial tissue, which is found in the nasopharynx, palatine tonsils, and base of the tongue [3]. However, anatomical MR and CT imaging is also limited in this area because lymphoepithelial tissue takes up contrast and is hyperintense on T2-weighted images, and a tumor might be unnoticed therein. One possible solution for this dilemma is the use of diffusion-weighted imaging (DWI) as part of a PET/MR protocol [4–7]. The cellularity of a tumor generates a low apparent diffusion coefficient (ADC), representing a contrast to normal lymphoepithelial tissue (Fig. 2).

The FDG uptake of a tumor is quantified at most institutions as part of clinical routine [3]. This may be helpful for following up the patient after radiation therapy or chemotherapy. No definitive threshold of the standard uptake value (SUV) exists for the differentiation of benign tissue and malignant tumors, for the differentiation of low-grade and high-grade lesions, or for prognostication [3, 8–14].

Due to less interference of artifacts from dental hardware, PET/MR is supposedly advantageous in the suprahyoid neck, whereas PET/CT is less prone to movement and swallowing artifacts occurring in the infrahyoid neck [15]. New MR reconstruction algorithms aiming at metal artifact reduction might further enhance the use of MR in the oral cavity [16].

Hybrid imaging is not routinely performed for the initial staging of patients with small tumors or if there is no clinical suspicion for nodal metastatic disease. Many centers perform sentinel node single-photon emission computed tomography/computed tomography (SPECT/CT) imaging using radiolabeled nanocolloids for the assessment of the nodal stage in patients with oral cavity cancers and oropharyngeal cancers. The radiotracer is injected in peritumoral location, and hybrid lymphoscintigraphic images allow for sentinel node mapping and guide nodal biopsy [3]. Sentinel node biopsy is considered the only reliable presurgical approach for the identification of micrometastatic deposits in lymph nodes [3, 17, 18]. PET may be falsely negative for nodal involvement if metastatic lymph nodes are necrotic and have only a thin rim of viable tumor tissue or if they are cystic [3, 19] (Fig. 2). This is a common situation in patients with squamous cell carcinoma in the oral cavity and oropharynx, with cystic metastases being particularly related to the presence of human papillomavirus (HPV) subtypes 16 and 18, the latter to somewhat less extent. Therefore, the use of contrast-enhanced imaging techniques is advised in the staging of head and neck cancer patients. Cystic metastases may grow rapidly, and response to radiotherapy is sometimes limited (Fig. 3). One

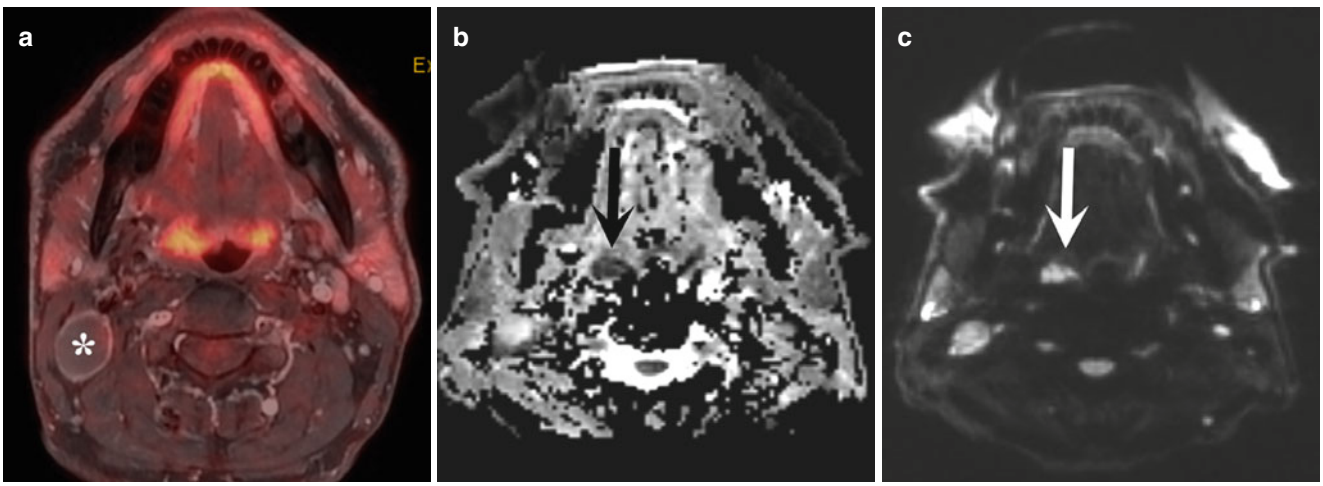

Fig. 2 Patient with palpable lump in the neck on the right side. A cystic lymph node metastasis with contrast enhancement of the rim (**a**, *asterisk*) is seen on FDG-PET/MR, but no obvious tumor. Diffusion-weighted imaging reveals a lesion with low apparent diffusion coefficient (**b**, *arrow*) and high signal on the b800 image (**c**, *arrow*) in the right tonsil. Subsequent tonsillectomy and histopathology confirmed a human papillomavirus (HPV)16-associated squamous cell carcinoma arising from the right tonsil

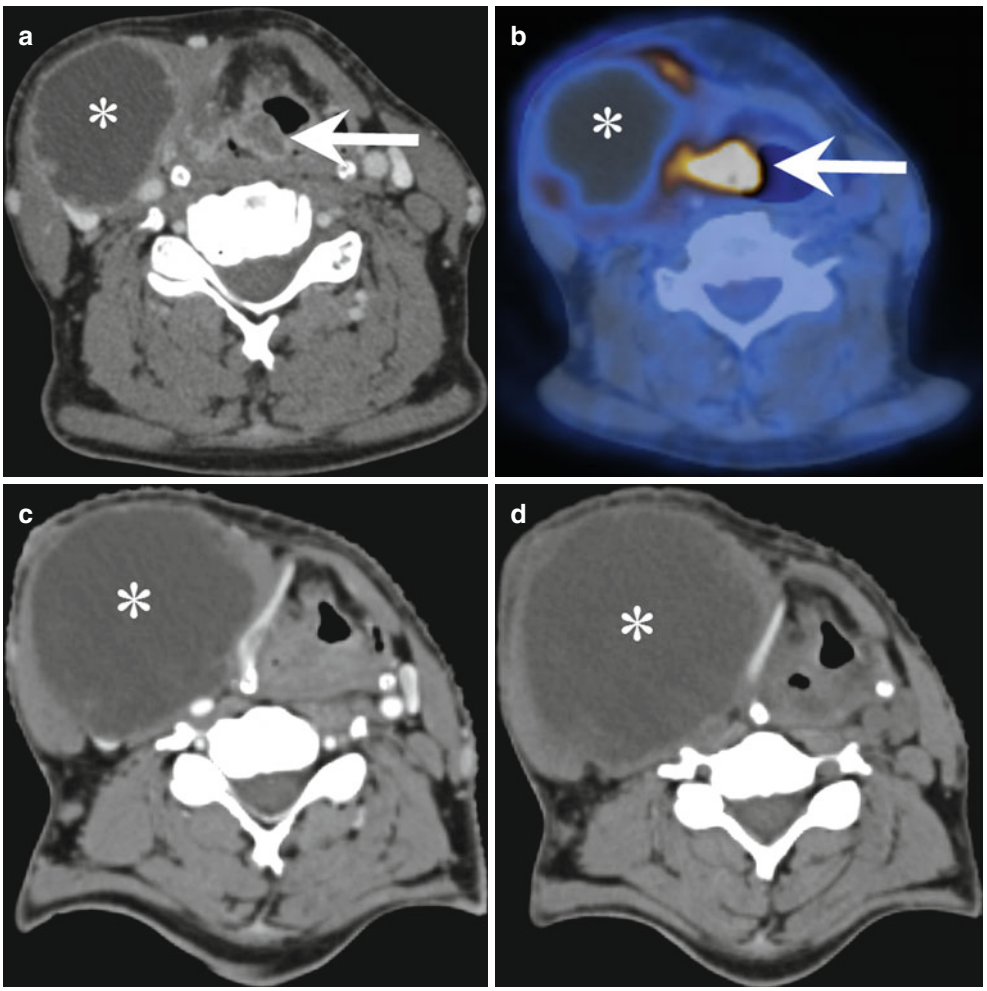

Fig. 3 HPV16-associated right-sided hypopharyngeal carcinoma. The tumor arises in the right piriform sinus and involves the right aryepiglottic fold (*arrows*), as seen on axial contrast-enhanced CT image (**a**) and FDG-PET/CT image (**b**). A large cystic metastasis (*asterisk*) with faintly FDG-avid rim is seen in the neck on the right side. Three weeks later the metastasis has grown in size (*asterisk*), as seen on the contrast-enhanced CT image (**c**). Another 6 weeks later, and after radiotherapy, the metastasis (*asterisk*) has increased even more (**d**)

rare differential diagnosis to cystic lymph node metastases with or without rim-like FDG uptake is branchial cleft cyst, which may be FDG-avid when infected, when containing lymphoid tissue, or when harboring neoplastic tissue [3, 20–22]. In large nodes without evidence of necrotic areas, lymphoma should be considered as a differential diagnosis. Unlike for the T staging, DWI as part of the PET/MR examination seems to offer no additional benefits for the N staging and provides rather redundant information [3, 7].

Extracapsular spread (ECS) on imaging refers to the macroscopic breach of the nodal capsule by tumor [3]. CT and MR may identify contour irregularities of the lymph node capsule (jagged or spiculated margins), stranding of the surrounding tissue, or even direct infiltration of surrounding structures by tumor [3, 23]. The presence of ECS depends on the size of lymph node metastases. ECS occurs in the majority of nodal metastases larger than 3 cm (approximately 75 %), in a significant number of metastatic nodes between 1 and 3 cm (up to 50 %), still in about one fifth of nodes less than 1 cm, and may rarely be present in clinically negative necks as well [3, 24–27]. ECS represents an adverse prognostic indicator, but its presence does not change the nodal stage.

The frequency of distant metastatic disease, mainly to the lung, increases with the T stage and with the N stage [3]. The presence of nodal metastases in the lower neck further increases the possibility of distant metastases. Hybrid PET/CT or PET/MR imaging is considered ideal for whole-body staging. PET/CT is the optimal hybrid modality for addressing the lung parenchyma. Lung imaging is somewhat problematic with PET/MR, because the lung parenchyma basically represents a black hole for MR. Several technical solutions have been suggested to overcome this drawback, e.g., breath-hold sequences and respiration-gated sequences [3, 15, 28]. The current threshold of lung nodule detection in clinical PET/MR ranges between 3 and 5 mm. However,

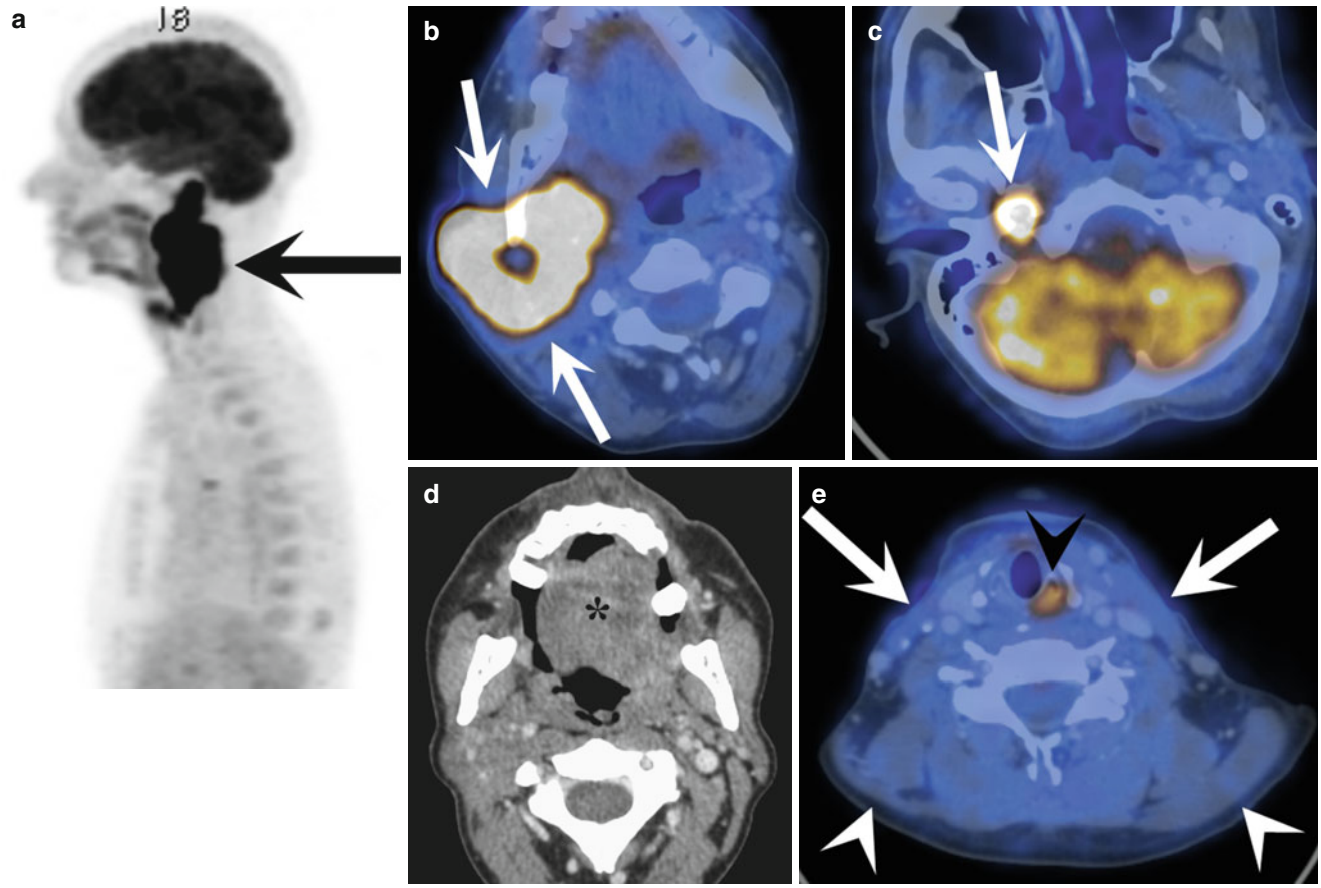

Fig. 4 Patient with cervical lymph node metastasis from an unknown primary tumor. Sagittal FDG-PET maximum intensity projection (MIP) image (**a**) shows an FDG-avid mass (*arrow*) in the neck, extending from the skull base to the level of the hyoid. The centrally necrotic mass (*arrows*) involves the parapharyngeal space, masticator space, and subcutaneous tissue on the right side, as seen on axial contrast-enhanced FDG-PET/CT image (**b**). The top of the mass (**c**, *arrow*) resides below the skull base at the level of the jugular foramen, which is infiltrated. Contrast-enhanced CT image (**d**) reveals an asymmetry of the tongue (*asterisk*), with right-sided atrophy. Contrast-enhanced FDG-PET/CT image (**e**) further reveals asymmetry of the trapezius muscles (*white arrow heads*) and sternocleidomastoid muscles (*arrows*), as well as right-sided loss of FDG uptake in the phonatory muscles (*black arrow head*). These findings are suggestive for combined neuropathy of the vagus nerve, accessory nerve, and hypoglossal nerve (constituents of Collet-Sicard syndrome along with glossopharyngeal nerve palsy)

there appears to be no need for dramatization of the probably somewhat inferior performance of PET/MR in lung nodule detection compared to PET/CT. In oncological patients, more than 98 % of FDG-negative subcentimeter lung nodules are benign, and 97 % of all lung nodules missed by PET/MR do not grow [29, 30]. Other common distant metastatic sites are the brain, the liver, and the bone. There, PET/MR might even offer advantages over PET/CT, particularly in the brain and in the liver, where high physiologic FDG uptake might obscure small metastases.

Several pitfalls need to be avoided in FDG-PET imaging of the head and neck. Physiologic FDG uptake occurs in a number of structures and in certain situations and should not be confused with pathology [3]. In children there is more FDG-avid lymphatic tissue in the adenoids, palatine tonsils, and lingual tonsils than in adults. Of the major salivary glands, the sublingual glands are usually most FDG-avid. Physiologic FDG uptake might also be encountered in the soft palate due to the abundance of salivary gland tissue there. Occasionally, the tip of the tongue appears FDG-avid. Uptake may also be seen in the orbicularis oris muscle and in muscles of mastication if patients were chewing during or shortly before the uptake phase. Depending on previous movement and muscle activity or if patients were positioned uncomfortably, uptake might be seen in the scalene muscles, sternocleidomastoid muscles, and prevertebral muscles. People who talked during the uptake phase have FDG-positive vocal cords and phonatory muscles. Unilateral FDG uptake in vocal cords, however, should raise the question for a lesion of the recurrent laryngeal nerve on the FDG-negative side or even complete vagal nerve palsy (Fig. 4).

Several benign lesions may be FDG-positive (Warthin's tumor, pleomorphic adenoma, schwannoma, branchial cleft cysts, inflammatory pseudotumor). On the other hand, some malignant tumors may be only faintly FDG-avid or even FDG-negative (adenocarcinoma of salivary glands, acinic cell carcinoma, chondrosarcoma, plasmacytoma).

Due to radiogenic inflammatory changes, FDG exams should be postponed to at least 3 months after therapy [3].

Local Staging

The radiological differential diagnosis for mucosal tumors is most often trivial, since the vast majority of tumors (more than 95 %) arising there is of squamous cell origin. The most common exception to that rule is lymphoma, which may arise from lymphoid tissue in Waldeyer's ring and may be accompanied by nodal disease in the neck. Lymphoma may be indistinguishable from squamous cell carcinoma based on morphological imaging characteristics. Its cellularity results in a low signal on T2-weighted images and a low apparent diffusion coefficient (ADC) on diffusion-weighted imaging (DWI). However, unlike carcinomas, lymphoma displaces rather than infiltrates surrounding healthy tissue. One exception to that rule is the somewhat frequent invasion of bone, which is seen in many lymphomas primarily arising in the head and neck. Additionally, lymphoma rarely exhibits intralesional areas of necrosis, appearing hyperintense on T2-weighted images, not even when lesions are large (Fig. 5). One important exception to that rule is posttransplant lymphoproliferative disorder (PTLD), which might show necrotic changes.

However, biopsy oftentimes precedes imaging, and histopathology already revealed the nature of the tumor when the patient is referred for radiological staging.

Throughout the upper aerodigestive tract, the TNM staging system is used to classify malignant tumors [31]. It represents the basis for treatment decisions, for prognostication, and for therapy response assessment.

Besides imaging-based classifications of tumor extent, there are other important factors that warrant consideration when the treatment plan for a patient is laid: patient's will, comorbidites, and life expectancy.

T Staging

The staging of tumor extent basically reverts to the discrimination of stage T4b tumors from tumors with lower T stages. This is because T4b tumors are considered not resectable, while all remaining tumors are generally believed amenable to surgical cure; some important exceptions applying (see below). Certainly, T4b tumors per se are technically resectable, but a surgical approach would result in a very poor outcome and severe functional disabilities of the patient. Items

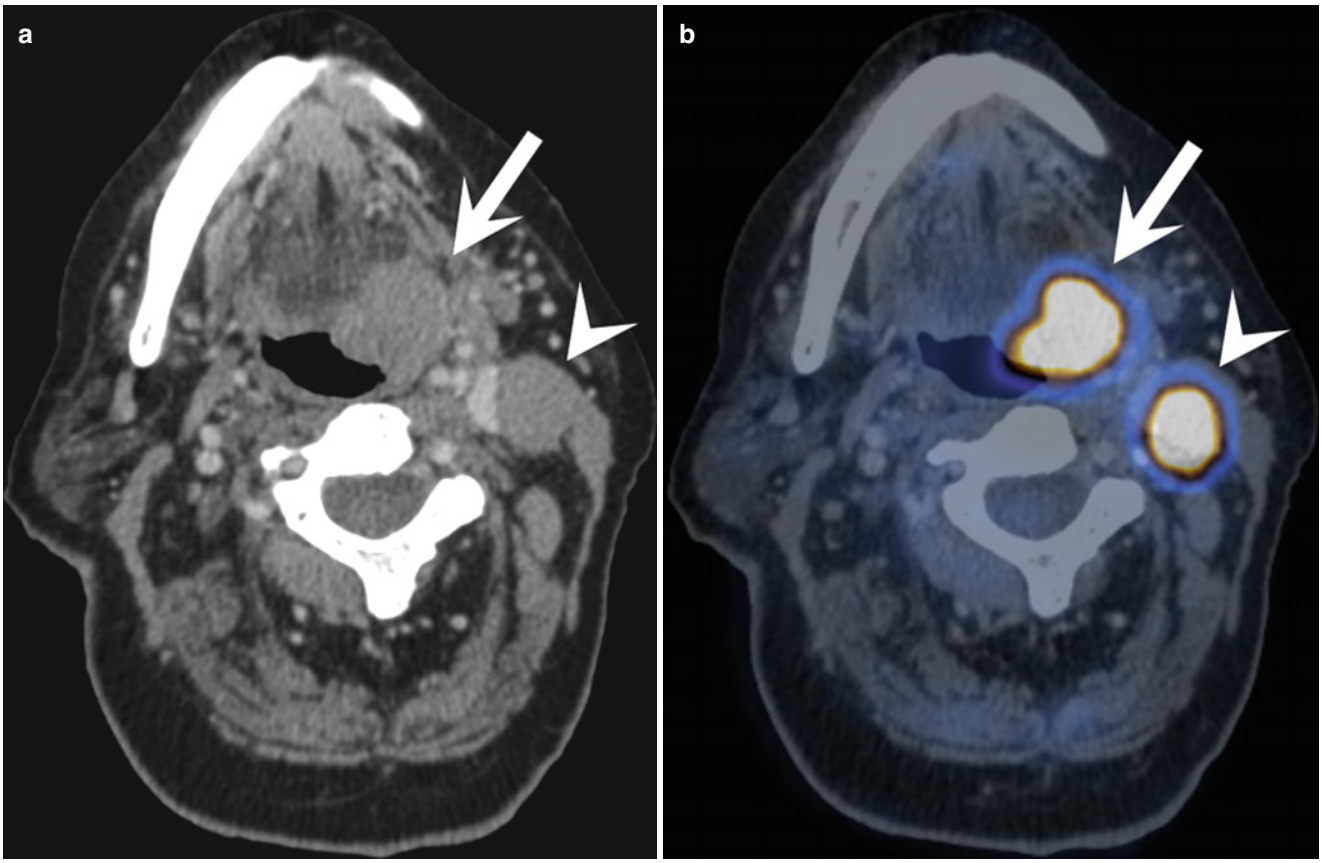

Fig. 5 Lymphoma arising in the left tonsil (**a**, *arrow*), involving the tongue base and the lateral wall of the oropharynx. An enlarged level II lymph node is seen on the left side (**a**, *arrow head*). Both lesions show a homogeneous density without evidence of necrosis, and intense FDG uptake (**b**, *arrow, arrow head*). These imaging features are not specific for lymphoma and may also be seen with squamous cell carcinoma

defining T4b stage are the same for all mucosal and extramucosal cancers of the head and neck, except for nasopharyngeal carcinoma where the T4 stage is not subdivided. Each one of the following three findings defines T4b stage and renders a tumor not resectable: infiltration of the prevertebral fascia and/or prevertebral muscles, encasement of the internal carotid artery or of the common carotid artery, and infiltration of the mediastinum. This general rule is slightly modified depending on the origin of the primary tumor. In the oral cavity and oropharynx, infiltration of the skull base, invasion of the pterygoid plates, and infiltration of the lateral pterygoid muscle are also defined as T4b stage. Additionally in the oropharynx, lateral extension into the nasopharynx is considered T4b. Although infiltration of the prevertebral space and/or the mediastinum is not explicitly mentioned in the T-staging system of oral cavity and oropharyngeal cancers, presence of these factors still would imply T4b stage. There is no breakdown of the T4 stage in T4a and T4b in the nasopharynx. T4 stage in the nasopharynx is defined as intracranial extension, involvement of cranial nerves, or extension into the orbit, masticator space, infratemporal fossa, or hypopharynx.

T4b-Defining Items

Infiltration of the Prevertebral Space

Such is given if the prevertebral fascia and/or muscles are infiltrated by a tumor. The clinical diagnosis is comparably easy, with unhindered motility of the posterior pharyngeal wall and the retropharyngeal contents (or a tumor) against the prevertebral fascial plane on palpation indicating absence of infiltration. The diagnosis on cross-sectional imaging is more difficult most of the time, unless continuous spread of tumor to the vertebral column is seen. The most suggestive feature is a complete obliteration of the prevertebral fat plane, which is better appreciated on non-fat-suppressed MR images than on CT. Other indicators of infiltration are an asymmetric thickening of muscles and contrast enhancement and FDG uptake of muscles (Fig. 6) [32, 33]. Since spillover artifact on PET may mimic tumor extension across the prevertebral fascia, correlation with morphological imaging is necessary.

Mediastinal Invasion

Mediastinal invasion is uncommon in head and neck cancer and if occurring is limited to laryngeal and hypopharyngeal carcinomas. Imaging characteristics of mediastinal invasion are an obliteration of the mediastinal fat with contrast enhancement, or FDG uptake with contiguous tumor. Also, asymmetric thickening, contrast enhancement, and FDG uptake of the wall of the mediastinal vessels and the esophagus should raise the suspicion for mediastinal infiltration by a tumor. Submucosal or mucosal infiltration of the proximal esophagus, which is comparably easy to resect, is difficult to differentiate from deeper invasion on imaging. If only the proximal 2 cm of the esophagus is involved, curative surgery is still considered possible by most surgeons. Such would revert to a stage T3 tumor (hypopharynx) or a stage T4a tumor (larynx).

Vascular Encasement

Vascular infiltration is assumed with circumferential tumor contact of 270° or more or if there is an irregular narrowing of the vessel due to contiguous tumor [34]. An obliteration of the fat plane between the vessel wall and a tumor has also a high positive predictive value [35]. In some instances of vascular infiltration, contrast enhancement and/or focal FDG uptake of the vessel wall is seen. However, these imaging findings may also be seen with peritumoral inflammatory infiltrates [36, 37].

Other T-Stage Issues

The classification of tumors into stages T1 to T4a is somewhat less pivotal than the differentiation of stage T4a and stage T4b tumors. Although the assignment of stages T1 to T4a impacts on the type of curative surgery the patient will undergo if qualifying, it does not primarily preclude surgery as with T4b tumors. Detailed tumor staging classifications by site are provided in Table 1.

There are, however, certain factors that are not necessarily part of the TNM staging system, but still might render a tumor not resectable, independently of its T stage. It is therefore as important as with T4b-defining factors to scrutinize the images for their presence. They consist of the following items: invasion of the laryngeal cartilage, invasion of the preepiglottic adipose tissue, perineural spread, orbital invasion, bone infiltration, skull base invasion, infiltration of the dura, and invasion of the brachial plexus [38].

Invasion of Laryngeal Cartilage

Owing to variable and often asymmetric ossification of the laryngeal cartilage, evaluation of tumor invasion is challenging with any cross-sectional imaging modality [3, 39]. Cartilage invasion is given with visible erosion or osteolysis of the cartilaginous skeleton on CT or MR or with permeative growth of tumor from the paraglottic to the paralaryngeal space (transmural extralaryngeal spread). It may also be assumed with contrast enhancement or focal FDG uptake of the cartilage; however, such might also be seen in chondroradionecrosis in a posttreatment setting, occurring in approximately 5 % of patients [40, 41]. Of note, sclerosis of the cartilaginous skeleton seen on CT does not necessarily indicate tumoral invasion, but might also represent reaction to contiguous tumor or postradiogenic change [3].

Invasion of Preepiglottic Adipose Tissue

Such may be assumed when the preepiglottic is obliterated or with contrast enhancement or focal FDG uptake in the preepiglottic space. The presence of erosion of the hyoid

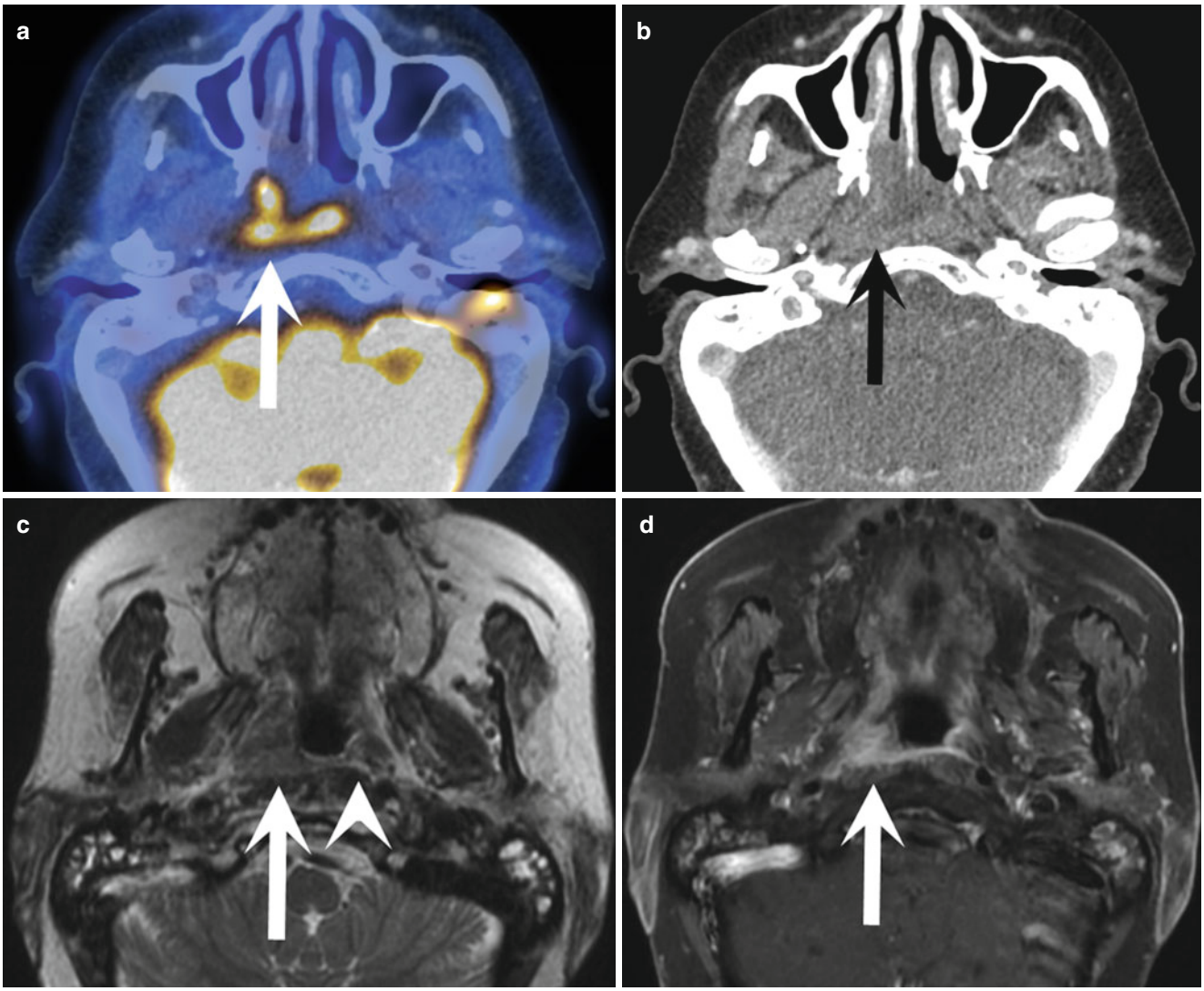

Fig. 6 Squamous cell carcinoma arising from the right-sided pharyngeal recess (fossa of Rosenmüller) with extension across the midline, as seen on contrast-enhanced FDG-PET/CT image (**a**, *arrow*). Presence of prevertebral invasion is difficult to assess on contrast-enhanced CT image because of low density contrast between tumor and prevertebral muscles (**b**, *arrow*). T2-weighted MR image (**c**) displays loss of the prevertebral fat plane on the right side (*arrow*), but preservation on the left side (*arrow head*). Contrast-enhanced T1-weighted fat-suppressed MR (**d**) further reveals a shaggy anterior margin of the right prevertebral muscles with contrast enhancement (*arrow*). MR features are suggestive of prevertebral invasion, which was confirmed with clinical examination

base is also a reliable indicator. Sagittal and/or axial T1-weighted non-fat-suppressed MR images are helpful due to signal intensity contrast between normal and infiltrated adipose tissue [42]. CT also provides reasonable density contrast in this region.

Perineural Spread

The combination of PET with contrast-enhanced MR is probably the best-suited imaging approach to perineural spread [3, 15, 43]. Features indicating perineural spread are thickening of nerves, contrast enhancement or FDG uptake along nerves, and loss of fat close to or within the foramina of the neurocranium or viscerocranium. The latter may be seen both with CT or MR, but MR is more sensitive. Post-gadolinium images with or without fat suppression may be used therefore. The first approach aims at eliminating the T1w-hyperintense signal of adipose tissue in regions below the skull base. However, this is often limited in the vicinity of air-containing spaces (nasal cavity, paranasal sinuses, mastoid air cells) due to field inhomogeneities elicited by local changes in magnetic susceptibility, e.g., paramagnetic properties of oxygen [44–46]. The second approach (without fat suppression) respects the fact that the neural foramina of the skull base are devoid of fat, and any T1w-hyperintense signal on post-gadolinium images should be regarded as potential tumor spread. Notably, enhancing tumor is seen as

Table 1 TNM staging system of head and neck cancers

		Oral cavity	Oropharynx	Hypopharynx	Larynx			Maxillary sinus	Nasal cavity, ethmoid sinus	Major salivary glands	Nasopharynx
					Supraglottis	Glottis	Subglottis				
Primary tumor	TX	Primary tumor cannot be assessed									
	T0	No evidence of primary tumor									
	Tis	Carcinoma in situ									
	T1	Tumor ≤2 cm (greatest dimension) Hypopharynx: and/or limited to 1 subsite of hypopharynx			Limited to 1 subsite of supraglottis, normal vocal cord mobility	Limited to vocal cords (± anterior or posterior commissure), normal vocal cord mobility T1a, 1 vocal cord; T1b, both vocal cords	Limited to subglottis	Limited to maxillary sinus mucosa	Limited to 1 subsite, ± bone invasion	Tumor ≤2 cm (greatest dimension)	Limited to nasopharynx/ extension to oropharynx or nasal cavity without parapharyngeal extension
	T2	Tumor >2 to ≤4 cm (greatest dimension) Hypopharynx: and/or extension to >1 subsite of hypopharynx or adjacent site			Invasion of more ≥1 supraglottic subsite/glottis/ adjacent region (e.g., base of tongue, vallecular, piriform sinus)	Extends to supraglottis and/or subglottis, vocal cord mobility impaired	Extends to vocal cords (normal or impaired mobility)	Invasion of hard palate, middle nasal meatus, anterior wall of maxillary sinus	Limited to 2 subsites, invasion of adjacent region within nasoethmoidal complex, ± bone invasion	Tumor >2 to ≤4 cm (greatest dimension)	Parapharyngeal extension
	T3	Tumor >4 cm (greatest dimension) Oropharynx: and/or extension to lingual surface of epiglottis Hypopharynx: and/or fixation of hemilarynx, extension to esophagus			Limited to larynx with vocal cord fixation Glottis: also invasion of paraglottic space, inner lamina of thyroid cartilage Supraglottis: also all of above + invasion of postcricoid area, preepiglottic space			Invasion of posterior wall of maxillary sinus, floor or medial wall of orbit, pterygoid fossa, ethmoid sinus, subcutaneous fat	Invasion of floor or medial wall of orbit, maxillary sinus, palate, cribriform plate	Tumor >4 cm (greatest dimension), extraparenchymal extension	Invasion of skull base, paranasal sinuses
	T4										Invasion of hypopharynx, orbit, masticator space (infratemporal fossa), intracranial extension, PNS along cranial nerves
	T4a	Invasion of adjacent structures (e.g., cortical bone, floor of mouth, maxillary sinus, skin of face)	Invasion of larynx, deep extrinsic tongue muscles, medial pterygoid muscle, hard palate, mandible	Invasion of thyroid cartilage, cricoid, hyoid, thyroid gland, central compartment (strap muscles, subcutaneous fat)	Invasion of outer lamina of thyroid cartilage, cricoid, invasion beyond larynx (e.g., trachea, deep extrinsic tongue muscles, strap muscles, thyroid, esophagus)			Invasion of anterior orbit, skin of face, pterygoid plates, sphenoid or frontal sinus Maxillary sinus: and/or infratemporal fossa, cribriform plate Nasal cavity, ethmoid sinus: and/or minimal invasion of anterior cranial fossa		Invasion of the skin, mandible, ear canal, PNS along facial nerve	
	T4b	Invasion of masticator space, pterygoid plates, skull base, encasement of ICA	Invasion of lateral pterygoid muscle, pterygoid plates, lateral nasopharynx, skull base, encasement of ICA	Invasion of prevertebral space, mediastinum, encasement of ICA				Invasion of orbital apex, dura, brain, middle cranial fossa, nasopharynx, clivus, PNS along cranial nerves other than $N.V_2$		Invasion of skull base, pterygoid plate, encasement of ICA	

Regional lymph nodes	NX	Regional lymph nodes cannot be assessed	
	N0	No evidence of regional lymph node metastasis	
	N1	1 ipsilateral lymph node metastasis ≤3 cm (greatest dimension)	Unilateral lymph node metastasis ≤6 cm (greatest dimension) above supraclavicular nodes, unilateral or bilateral retropharyngeal lymph node metastasis ≤6 cm (greatest dimension)
	N2	Ipsilateral, contralateral, bilateral lymph node metastasis >3 to ≤6 cm (greatest dimension)	Bilateral lymph node metastases ≤6 cm (greatest dimension) above supraclavicular nodes
	N2a	1 ipsilateral lymph node metastasis >3 cm to ≤6 cm (greatest dimension)	
	N2b	>1 ipsilateral lymph node metastasis ≤6 cm (greatest dimension)	
	N2c	Bilateral/contralateral lymph node metastasis ≤6 cm (greatest dimension)	
	N3	≥1 lymph node metastasis >6 cm (greatest dimension)	N3a: Lymph node metastasis >6 cm N3b: Supraclavicular lymph node metastasis
Distant sites	M0	No distant metastasis	
	M1	Distant metastasis	

Adapted from Edge et al. [31]
Note: TNM staging of mucosal melanoma and thyroid malignancies is not provided. Major salivary glands include parotid, submandibular, and sublingual glands
ICA internal carotid artery, *PNS* perineural spread

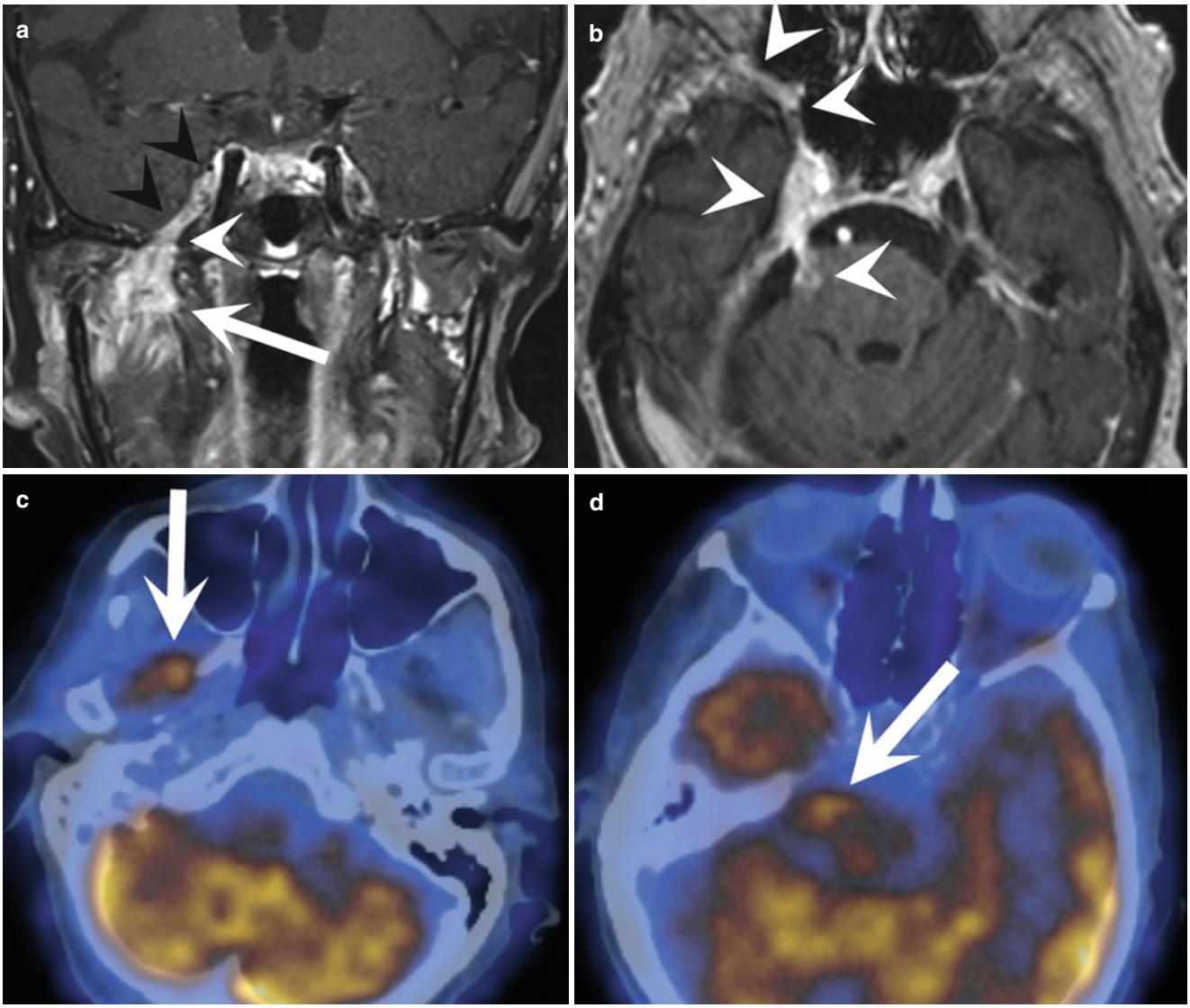

Fig. 7 Patient with right-sided facial nerve palsy and pain in the cheek. Contrast-enhanced T1-weighted fat-suppressed coronal MR image (**a**) shows a tumor in the deep lobe of the right parotid gland (*arrow*). The mandibular nerve is thickened and enhances (*black arrow heads*) along its course from the cavernous sinus via the foramen ovale (white arrow head) to the masticator space. Axial contrast-enhanced T1-weighted coronal MR image (**b**) confirms extensive perineural spread (*arrow heads*) along the trigeminal nerve and its branches, invading the infraorbital canal, foramen rotundum, cavernous sinus, Meckel's cave, prepontine cistern, and mid pons at the level of the root exit zone of the trigeminal nerve. FDG-PET/CT images reveal uptake in the right-sided masticator space, pronounced in the location of the mandibular nerve (**c**, *arrow*), as well as in the right-sided prepontine cistern and pons (**d**, *arrow*)

intermediate to bright signal, and non-infiltrated fat retains its very bright signal, which helps in differentiating both instances despite the absence of fat suppression [44, 45]. Another feature indicating perineural spread is a widening of foramina or canals of the skull base, although this is rather considered a late event [47].

In most patients, perineural spread is already symptomatic by the time it becomes evident on cross-sectional imaging [3, 46]. However, clinically evident perineural spread is often missed by FDG-PET/CT imaging, particularly if the disease burden is relatively small and if the radiologist is not familiar with the anatomy of the skull base and the course of the cranial nerves. The presence of perineural spread in a patient generally predicts a poor outcome (Fig. 7). Although adenoid cystic carcinoma is notorious for its propensity to spread along nerves, due to the overwhelming predominance of squamous cell histology in head and neck cancer (more than 95 %), perineural spread is most commonly seen with squamous cell carcinoma.

Perineural spread refers to the macroscopic extension of tumor along a nerve and does necessarily imply growth along the perineurium itself [3]. The nerve serves as a highway and allows the tumor, representing a hitchhiker, to travel away from its original site, taking an unexpected route that may

lead to distant sites, sometimes far beyond the region of planned surgical resection or irradiation [3, 44, 48]. This may alter or even foil the treatment plan. In the head and neck, perineural spread most often occurs along major branches of the trigeminal nerve (maxillary nerve, foramen rotundum; mandibular nerve, foramen ovale; inferior alveolar nerve, mandibular canal) and facial nerve (stylomastoid foramen), with the auriculotemporal nerve (behind the neck of the mandible) representing a shortcut between the mandibular nerve and the facial nerve as well as the glossopharyngeal nerve. Perineural spread may occur in an antegrade fashion, in a retrograde fashion, or in both fashions at the same time [45, 46, 48]. If advanced perineural spread is encountered, sometimes contiguous meningeal infiltration is seen, starting at the involved skull base foramina, or even direct infiltration of the brainstem at the level of the root entry/exit zones (Fig. 7).

The coexistence of imaging signs of accessory nerve infiltration, such as asymmetry of the sternocleidomastoid muscles and the trapezius muscles, and recurrent laryngeal nerve involvement, such as asymmetry of the vocal cords and lack of FDG uptake in phonatory muscles of the affected side, or vagus nerve involvement, such as unilateral relaxation of the soft palate, should prompt the search for a central lesion that could cause simultaneous accessory nerve and vagus nerve palsy (Fig. 4). Such lesions most of the time are lymph node metastases with extracapsular extension below the skull base. Sometimes, a nasopharyngeal cancer directly infiltrates this deep. Another possibility would be a bone metastasis extending into the jugular foramen. Primary lesions arising at the level of the jugular foramen (glomus tumos, schwannomas, meningiomas) occasionally elicit such symptoms. The constellation of palsies of the accessory nerve, vagus nerve, and glossopharyngeal nerve is termed Vernet syndrome; the latter palsy (N.IX) usually yields no specific imaging signs and is unapparent. If also the hypoglossal nerve is involved, this is then termed Collet-Sicard syndrome. One-sided atrophy and/or fatty degeneration of the tongue represents the imaging correlates for unilateral hypoglossal nerve palsy.

Orbital Invasion

Such is assumed with obliteration of the orbital fat planes or with contrast enhancement or FDG uptake within the orbital adipose tissue. One important pitfall here is spillover of FDG activity from the external ocular muscles, especially if patients did not close their eyes during uptake and acquisition or when a mismatch of PET and CT or MR images is present [3]. Another uncommon pitfall in irradiated or postoperative patients is myositis, which may also lead to a thickening, contrast enhancement and FDG uptake of external ocular muscles (Fig. 8). Lytic destruction of the medial wall or floor of the orbit also suggests orbital invasion, but due to the thin bone there, might be difficult to differentiate from bone atrophy due to tumoral compression, if no soft tissue mass is seen extending beyond the osseous confines into the orbit. Notably, it should be differentiated if only the medial orbital wall is invaded or if there is invasion of the anterior orbit or even tumor extent into the apex, with the latter item indicating T4b stage. Further differentiation into extraconal or intraconal disease and relation of tumor to the optic nerve represent valuable information for the referring clinician.

Bone Infiltration

This is seen by erosion of bone on CT; by loss of fat-equivalent signal intensity or density on MR or CT, respectively; and by contrast enhancement on CT or MR [49]. Focal FDG uptake of bone usually also indicates bone infiltration, but might also be seen in instances of postradiogenic osteonecrosis. Generally, bone infiltration is best assessed with thin-slice CT images, reconstructed with a sharp kernel in bone window display. As said above, bone infiltration by a tumor might be hard to appreciate in regions where the bone is thin and when no soft tissue mass is seen extending beyond the bone. Invasion of the medullary cavity of bone is easily assessed with MR due to its intrinsic high soft tissue contrast that visualizes changes of signal intensity, with fatty marrow being replaced by T1w-hypointense and T2w-hyperintense tumor. However, superficial erosion of bony cortex is difficult to determine with conventional MR pulse sequences due to the paucity of hydrogen molecules in this tissue. The event of PET/MR has stimulated the demand for MR pulse sequences capable of exactly delineating bony cortex for attenuation correction purposes. Such novel MR pulse sequences often use extremely short echo times and are termed ultrashort echo time (UTE) sequences or zero echo time (ZTE) sequences [50–53].

Skull Base Invasion

Both MR and CT are widely used to address skull base invasion, however, with different advantages and disadvantages. Due to the anatomy of the skull base, erosion of the bone is sometimes missed on CT imaging, while MR may be more sensitive and show signal changes in the spongiosa induced by tumor. Another advantage of MR is the absence of beam-hardening artifacts elicited by skull base bones [54–56]. On the other hand, MR might be falsely negative where the skull base is thin and no cancellous bone exists, whereas CT shows lytic changes of the thin cortical bone. Contrast enhancement and FDG uptake of the skull base may also be noted. Spillover of activity from FDG-avid brain is considered an important pitfall here [3]. Other findings indicating skull base invasion are widened foramina and canals.

Infiltration of the Dura

A nodular thickening of the dura, contrast enhancement, or FDG uptake of the dura may indicate dural infiltration by a tumor. Linear thickening or contrast enhancement might also be seen as a reaction to contiguous tumor after radiation therapy, or after surgery in the vicinity of the

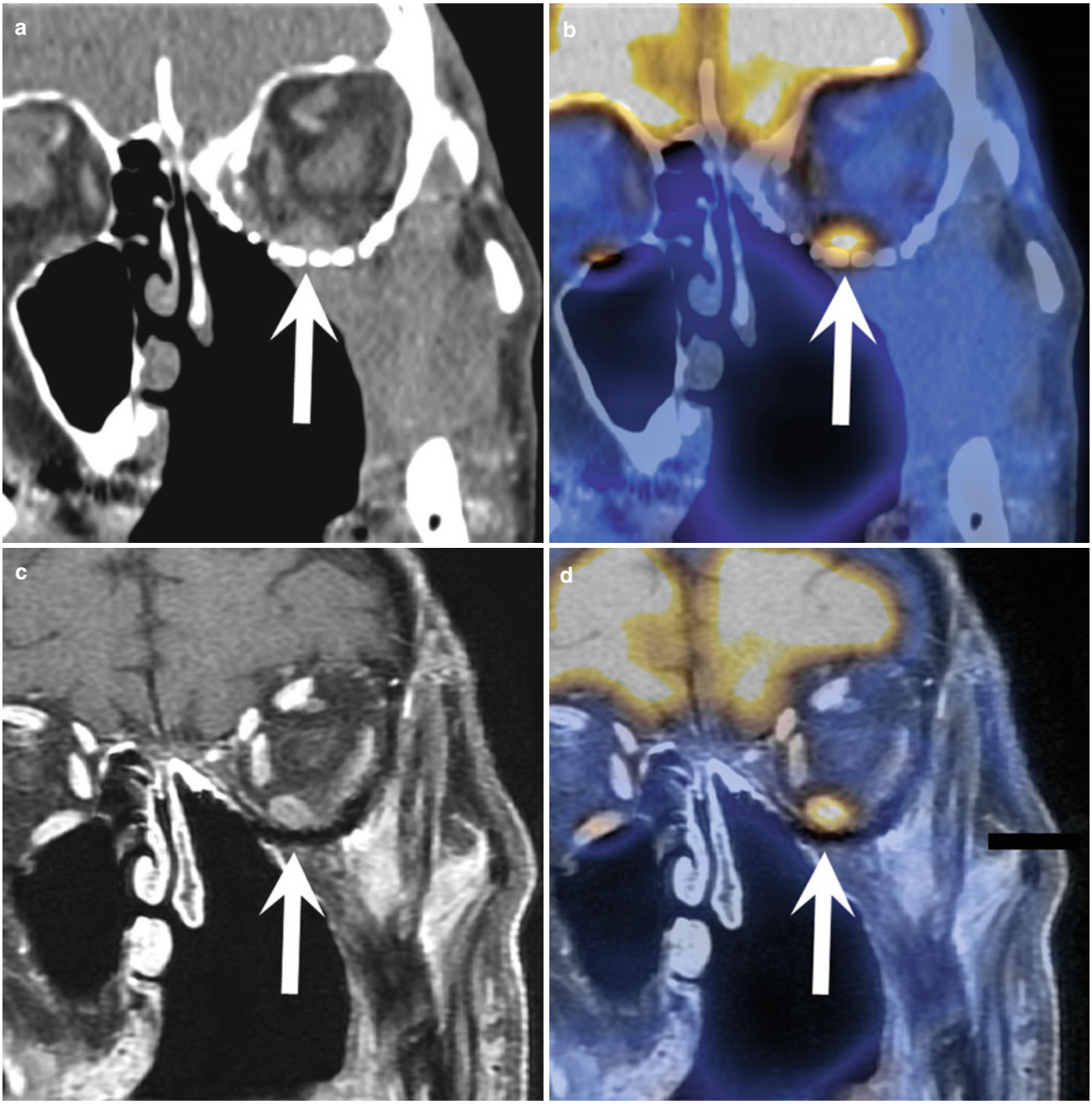

Fig. 8 Follow-up imaging after radiotherapy and reconstruction of the floor of the left orbit, which was infiltrated by a maxillary sinus carcinoma. An FDG-avid mass is seen in the orbit right above the reconstructed floor with surrounding stranding of the intraconal and extraconal adipose tissue on coronal CT image (**a**, *arrow*) and coronal FDG-PET/CT image (**b**, *arrow*). Contrast-enhanced fat-suppressed coronal MR image (**c**, *arrow*) and FDG-PET/MR image (**d**, *arrow*) lead to the diagnosis of myositis of the inferior rectus muscle and no evidence of local tumor recurrence along the reconstructed orbital floor

surgical access path. More widespread nodular dural enhancement is usually seen with infectious, inflammatory, granulomatous, and idiopathic causes of pachymeningitis or with normal pressure hydrocephalus, which might incidentally coexist in head and neck cancer patients and represent a differential diagnosis to dural involvement by a tumor. Dural infiltration is best assessed using contrast-enhanced MR. Due to the close relationship of dura and FDG-avid brain, PET may have difficulties in recognizing increased FDG uptake of the dura (Fig. 9). Close to the skull base, CT is oftentimes limited by beam-hardening artifacts [54–56].

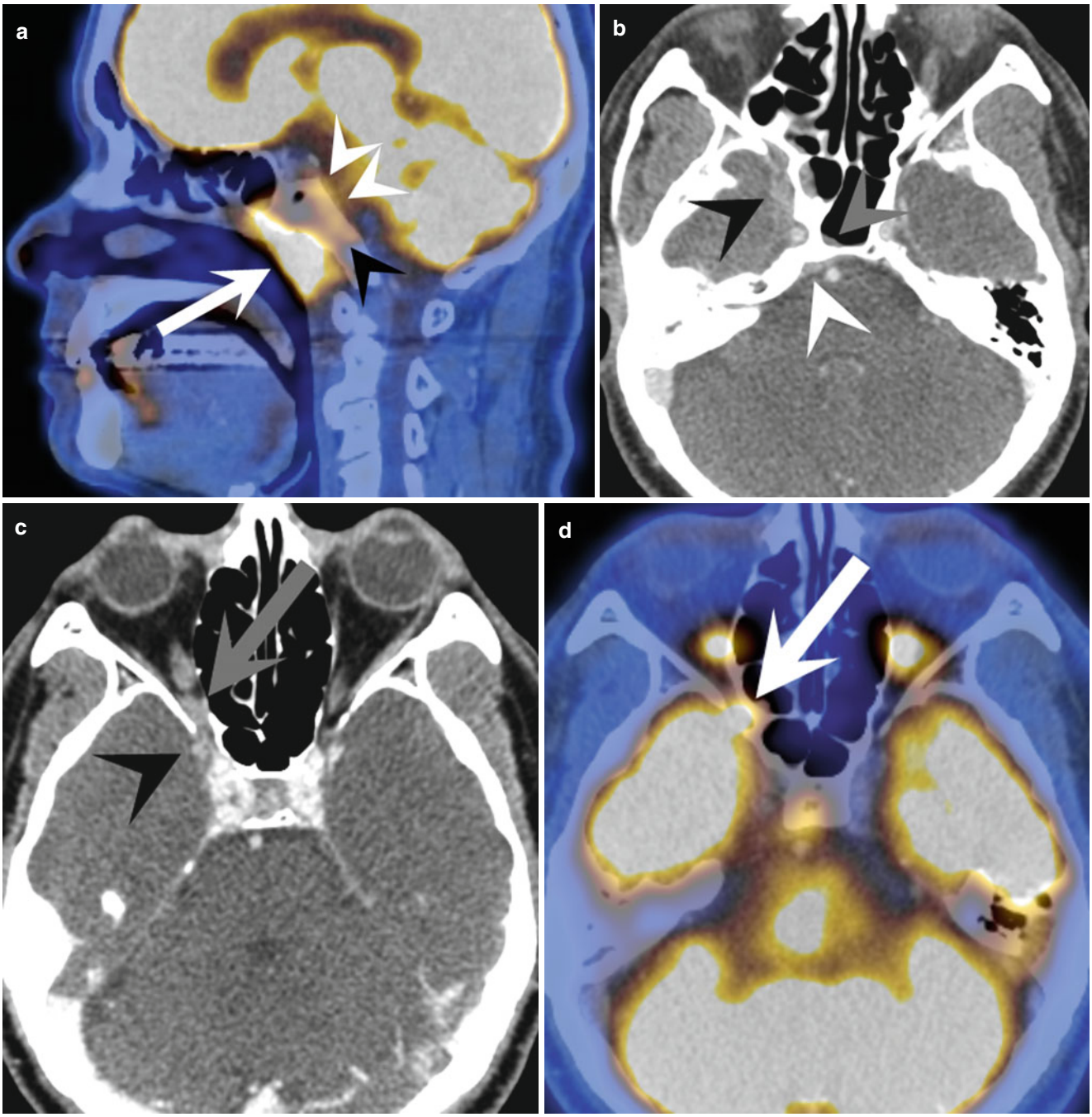

Fig. 9 Patient with EBV-associated poorly differentiated nasopharyngeal carcinoma. Sagittal contrast-enhanced FDG-PET/CT image (**a**) shows the tumor (*arrow*) extending from the nasopharynx via the clivus (*black arrow head*) to the epidural space in retroclival location (*white arrow heads*). Retroclival epidural invasion is also seen on axial contrast-enhanced CT image (**b**, *white arrow head*), as well as extension into the sphenoid sinus (*gray arrow head*) and dural infiltration in the middle cranial fossa (*black arrow head*), lateral and inferior to the cavernous sinus. Axial contrast-enhanced CT image (**c**) (a few slices above the plane of image b) reveals that the temporal dural infiltration (*arrow head*) is in continuation with the foramen rotundum and inferior orbital fissure, where tumor is seen extending into the orbit (*arrow*). Intraorbital extension on the right side is also appreciated on axial contrast-enhanced FDG-PET/CT image (**d**) as FDG-avid mass (*arrow*). However, dural invasion is obscured by activity spillover from FDG-avid brain

Invasion of the Brachial Plexus

Thickening of nerves, obliteration of fat between trunks, divisions, and cords of the plexus, as well as contrast enhancement and FDG uptake along nerves might indicate tumor extending into the brachial plexus. Contrast-enhanced MR (or PET/MR) is the modality of choice.

Sites and Subsites in the Head and Neck

Besides the extension into the deep, i.e., the infiltration of neighboring anatomical structures and spaces, also the longitudinal extension of tumor into other sites or subsites of the head and neck is important for staging and pretherapeutic assessment.

Almost all mucosal sites of the head and neck have subsites, whose infiltration impacts on the T stage (Fig. 10).

The oral cavity has nine distinct subsites: the upper lip, the lower lip, the anterior two thirds of the tongue (posterior one third is an oropharyngeal subsite), the floor of the mouth, the upper alveolar ridge, the lower alveolar ridge, the retromolar trigone, the hard palate, and the buccal mucosa. Some authors address the lips and alveolar ridges as single subsites each, which makes a total of seven subsites. The size of the tumor mainly defines the T stage, whereas the involvement of subsites plays a role in surgical planning (Table 1).

The oropharynx comprises five subsites: the posterior one third of the tongue including the tongue base, the soft palate including the uvula, the palatine tonsils together with the tonsillar pillars, the posterior and lateral oropharyngeal wall, and the valleculae. Some authors also consider the lingual surface of the epiglottis part of the oropharynx. As in the oral cavity, tumor size matters most in the T staging, while the involvement of subsites impacts on surgical planning (Table 1).

The situation is different in the hypopharynx. Here, invasion of subsites is critical for accurate T staging (Table 1). The hypopharynx has six subsites: the left and right piriform sinus, the postcricoid area (the pharyngoesophageal junction), the left and right lateral hypopharyngeal wall, and the posterior hypopharyngeal wall.

The supraglottic larynx has five distinct subsites: the vestibular folds (false vocal cords) and the sinus of Morgagni (upper laryngeal ventricle), the arytenoid cartilages, the suprahyoid portion of the epiglottis, the infrahyoid portion of the epiglottis, and the aryepiglottic folds.

In the glottis, there are three subsites: the true vocal cords together with the glottis muscles, the anterior commissure, and the posterior commissure.

The subglottis is the larynx portion inferior to the true vocal cords, extending from 5 mm below the free margin of the true vocal cords to the inferior margin of the cricoid cartilage. The subglottis has no separate subsites.

In the nasal cavity and paranasal sinuses, subsites are the septum, the floor, the lateral wall and the vestibule of the nasal cavity, the right and left maxillary sinus, and the right and left ethmoid sinus. The lateral wall of the nasal cavity includes the three turbinates, the ostiomeatal complex, and the nasolacrimal duct.

In the nasopharynx, subsites are not important for the T staging, but play a role in presurgical assessment. Subsites of the nasopharynx are the vault, the posterior nasopharyngeal wall, and the lateral nasopharyngeal wall, which consists of the torus tubarius (eustachian tube opening) anteriorly and the pharyngeal recess (fossa of Rosenmüller) posteriorly.

N Staging

Nodal Levels

The presence and extent of nodal metastases directly affect patient management [3].

On cross-sectional imaging, nodal levels in the neck are assigned according to the classification of Som et al., which represents an imaging-based correlation with clinically based nodal classifications [57]. Relevant anatomical structures, which serve as orientation for level borders, are the jugular fossa, the inferior border of the corpus of the mandible, the mylohyoid muscle, the anterior belly of the digastric muscle, the posterior boundary of the submandibular gland, the internal jugular vein, the common carotid artery and internal carotid artery, the lower border of the hyoid bone, the anterior and posterior boundary of the sternocleidomastoid muscle, the anterior boundary of the anterior scalene muscle, the lower margin of the cricoid cartilage, the upper margin of the clavicle, and the top of the manubrium sterni.

Fig. 10 Patient with clinical suspicion of a carcinoma of the tongue on the left side. Sagittal FDG-PET MIP image (**a**) shows an FDG-avid lesion (*arrow*) in the oral cavity. Axial FDG-PET/CT image (**b**) confirms the presence of an FDG-avid tumor (*arrow*) in the sublingual space the left side. The true extent of the tumor (*arrow heads*) is somewhat hard to identify on the contrast-enhanced CT image (**c**). Contrast-enhanced CT (**d**) image at the level of the body of the hyoid bone reveals size asymmetry of the submandibular glands (*arrows*), but no pathologic FDG uptake is seen on corresponding FDG-PET/CT image (**e**, *arrows*). The extent of the tumor in the tongue and sublingual space is clearly better identified on axial fat-suppressed T2-weighted MR image (**f**, *arrow heads*); the lingual septum is preserved. Axial and coronal fat-suppressed T2-weighted MR images (g and h, respectively) at the level of the sublingual glands shows dilation of Wharton's duct on the left side (*arrow*) (**h**). This is suggestive for tumor extension into the floor of the mouth, as seen on coronal fat-suppressed T2-weighted MR image (**i**) which reveals the craniocaudal dimension of the tumor (*arrow heads*) arising from the sublingual space (*arrow*). This was a sublingual carcinoma stage T2, extending into the tongue. Infiltration of the floor of the mouth would render a tongue carcinoma stage T4a

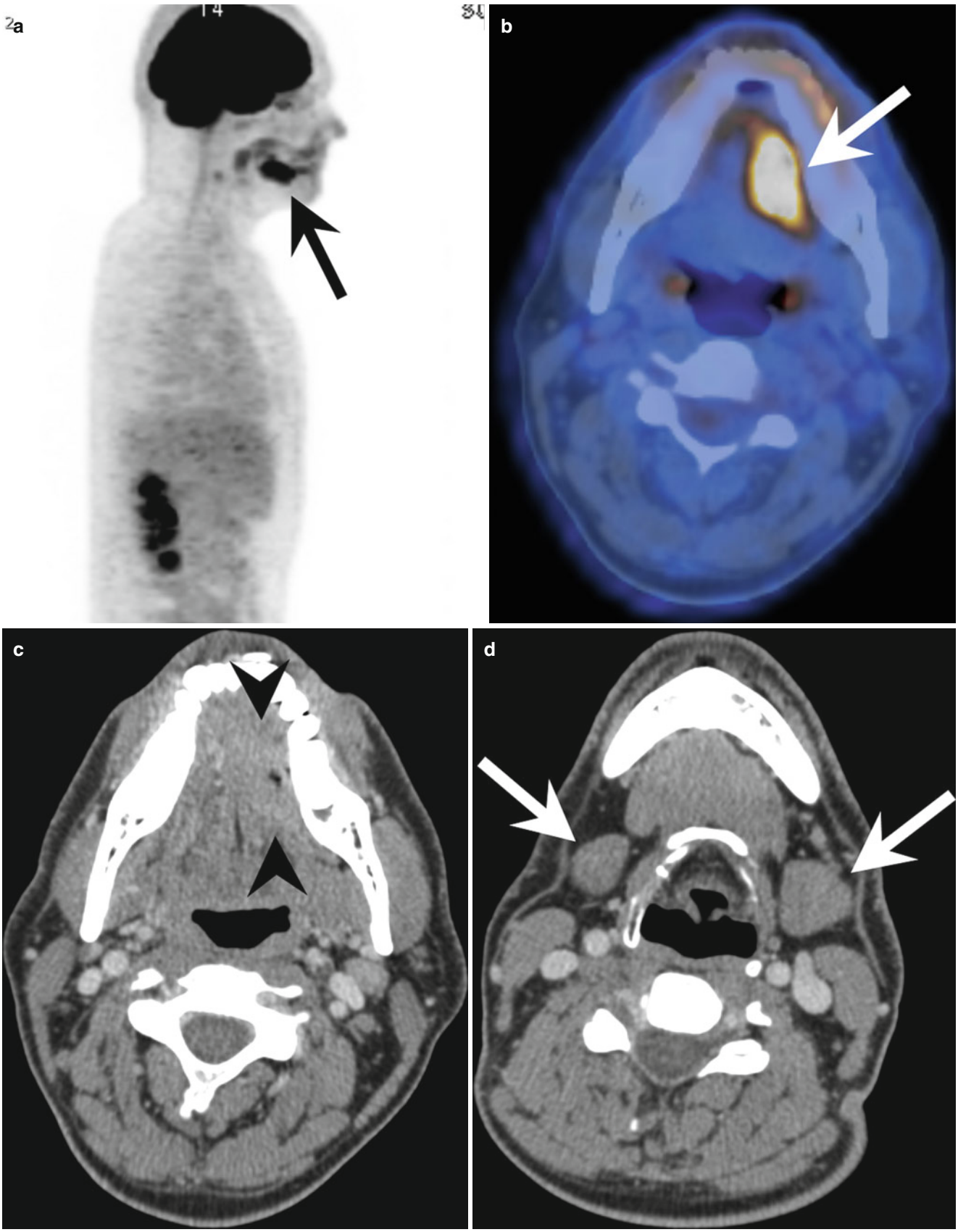
a
b
c
d

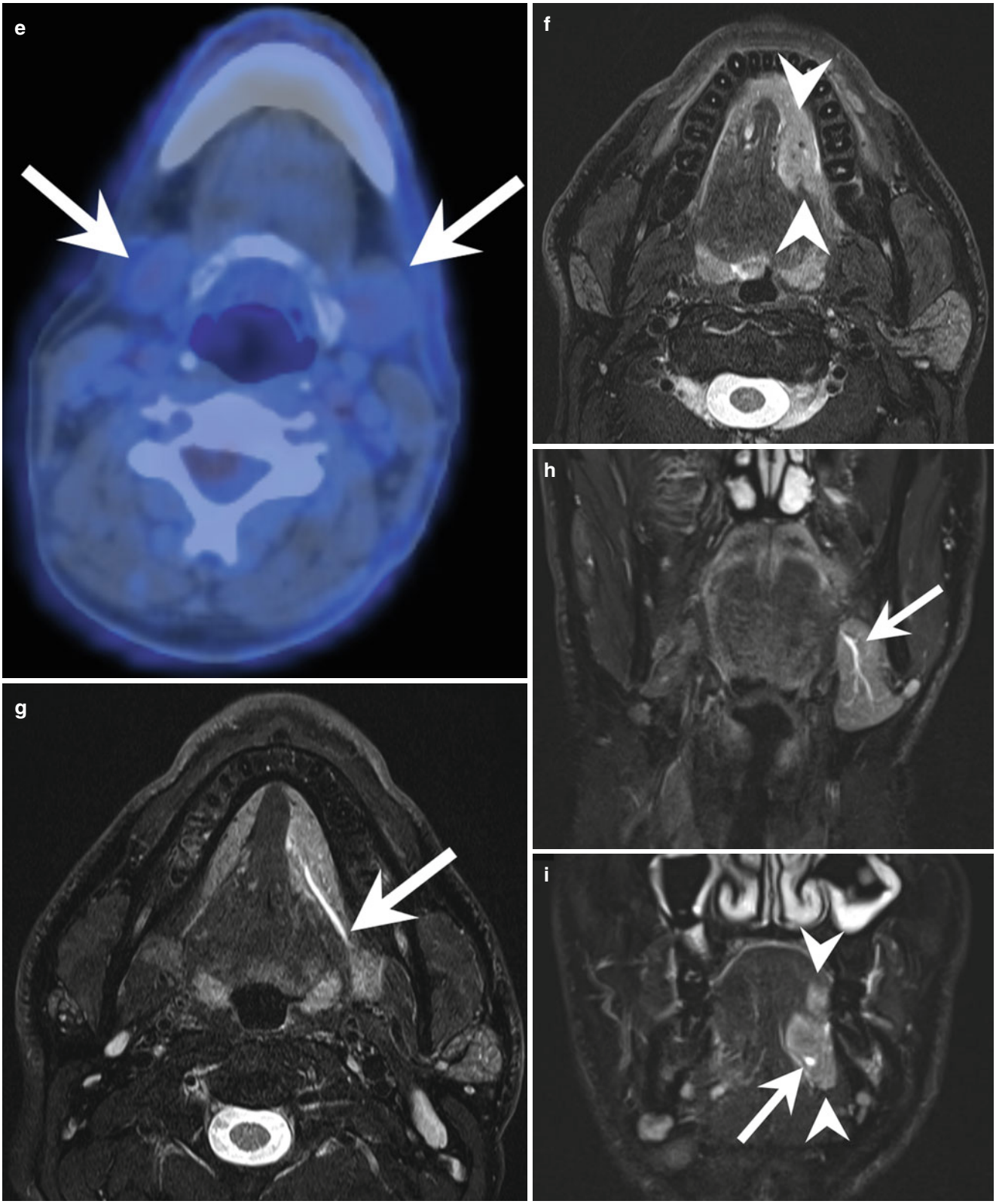

Fig. 10 (continued)

Level I: These nodes are located below the mylohyoid muscle and above the inferior margin of the hyoid. The posterior boundary of the submandibular gland represents the posterior border of level I. Level IA nodes (submental nodes) are found around the midline between the anterior bellies of both digastric muscles. Level IB nodes (submandibular nodes) are located lateral to the anterior bellies of both digastric muscles.

Level II: These nodes are part of the internal jugular chain which is also referred to as deep cervical lymph node chain. Level II extends from the base of the skull unto the inferior border the hyoid bone. The anterior border of level II is the posterior boundary of the submandibular glands, and its posterior border is represented by the posterior boundary of the sternocleidomastoid muscle. Level II is divided into IIA and IIB by the accessory nerve; since this structure is not identified on imaging, the internal jugular vein serves as an alternative. Level IIA nodes are located anteriorly, laterally, or medially to the internal jugular vein. Level IIB nodes are located posteriorly to the internal jugular vein unless inseparable, then being considered level IIA nodes by most authors. Some authors consider retropharyngeal nodes as part of level IIA.

Level III: Between the inferior margin of the hyoid bone and the inferior margin of the cricoid cartilage, the internal jugular chain or deep cervical lymph node chain continues in level III. The posterior boundary of the sternocleidomastoid muscle represents the posterior border of level III, and its medial border is defined by the medial margins of the common carotid artery and internal carotid artery. These two arteries also represent the anterior border of level III.

Level IV: From below the inferior margin of the cricoid cartilage unto the superior border of the clavicle, the internal jugular chain or deep cervical lymph node chain continues in level IV. As with level III, the medial and anterior borders of level IV are defined by the margins of the common carotid artery. The posterior border of level IV is defined by the oblique line extending from the posterior edge of the sternocleidomastoid muscle to the posterior edge of the anterior scalene muscle.

Level V: This level contains the posterior neck triangle lymph nodes. Some authors divide it into VA and VB with respect to the inferior margin of the cricoid cartilage, although this is usually not important for surgery. Level V extends behind levels II–IV from the skull base to the level of the clavicle.

Level VI: This level contains pretracheal, paratracheal and prelaryngeal (Delphian) nodes, which are located anterior to the visceral space. Level VI is located anterior to levels III and IV, being separated by the internal carotid artery and common carotid artery. It extends from the inferior margin of the hyoid bone to the top of the manubrium sterni.

Level VII: Lymph nodes in this level are located in the superior mediastinum between the two common carotid arteries, and below the top of the manubrium sterni.

Some important nodal groups are not included in this system, such as the intraparotid lymph nodes, the preauricular lymph nodes, and the facial lymph nodes.

Implications for Nodal Staging

Nodal levels play an important role in pretherapeutic planning, but are not part of the TNM staging system. With the exception of nasopharyngeal cancer, the exact anatomical distribution of nodal metastases in the neck is not important for the N stage. The presence of supraclavicular (considered level IV by most authors) lymph node metastases indicates an N3 stage in nasopharyngeal cancer. In all other carcinomas, only size (smaller than 3 cm, between 3 and 6 cm, larger than 6 cm), number, and laterality (ipsilateral, contralateral, bilateral) of nodal metastases define the N stage (Table 1).

Oral cavity carcinomas mainly metastasize to lymph nodes in levels I through III. Drainage from the lip is bilateral. Level IA nodes receive lymphatic afferences from the central part of the lower lip, the apex of the tongue, and the floor of the mouth. Their drainage is to level IB nodes and level IIA nodes.

The tributaries of level IB are the cheek, the side of the nose, the region of the canthus, the lips except the medial part of the lower lip, the alveolar ridges, the hard palate, and the anterior two thirds of the lateral aspect of the tongue. Carcinomas arising in the retromolar trigone and floor of the mouth have the highest predilection of nodal involvement (approximately 50 %), followed by the oral part of the tongue (approximately 40 %) [58]. Nodal involvement is least common in cancers of the lip.

Oropharyngeal carcinomas disseminate usually to the internal jugular chain (in levels II and III) and retropharyngeal lymph nodes. Overall, two thirds of patients with oropharyngeal carcinomas present with cervical lymph node metastases, with the base of the tongue having the highest frequency, followed by the palatine tonsils, the oropharyngeal walls, and the soft palate and uvula [3, 58].

The hypopharynx has a rich lympathic network and drains through the thyrohyoid membrane to level IIA and level III nodes and to level V nodes to some less extent. The posterior pharyngeal wall typically tributes to lymph nodes below the jugulodigastric node. If the tumor involves the lowest portion of the hypopharynx, the pharyngoesophageal junction, lymphatic spread may occur to paratracheal (level VI) nodes.

Nodal drainage of the larynx varies by site. The supraglottis is derived from the buccopharyngeal anlage and has a rich lymphatic network. The glottis and subglottis are derived from tracheobronchial buds and have fewer lymphatic vessels [3]. Therefore, lymph node metastases are more often found with supraglottic tumors (more than 50 % have positive nodal stage,

20 % have bilateral nodal involvement), whereas the majority of glottic tumors present with stage N0 (Nodal involvement in stage T1 tumors, <2%; T2, 5% T3, 15–20 %; T4, 20–30 %). The main lymphatic pathway of the supraglottis is to levels II through IV. Since the true vocal cords are vastly devoid of lymphatics, nodal spread generally does not occur until the tumor has extended into the supraglottis or subglottis. In the subglottis there are one anterior lymphatic pedicle and two posterior lymphatic pedicles. The anterior one drains through the cricothyroid membrane into level III and IV or to level VI (prelaryngeal and pretracheal nodes). The posterior chain drains through the cricotracheal membrane to paratracheal lymph nodes (level VI).

Carcinomas in the nasal cavity have an incidence of approximately 10 % of nodal metastases at the initial presentation. Drainage of the vestibule is to level I nodes and facial and preauricular nodes. The paranasal sinuses are poor of lymphatic vessels. Nodal spread occurs usually not until the tumor has invaded the surrounding tissue. The first lymphatic station is the retropharyngeal chain.

In the nasopharynx, the vast majority of tumors present with lymph node metastases (approximately 90 %), which are bilateral in about half of tumors. The main drainage occurs to retropharyngeal lymph nodes.

Tumors arising in the parotid gland metastasize to intraparotid and periparotid lymph nodes, followed by an involvement of levels I through III. Submandibular gland malignancies mainly metastasize to levels I and II, followed by level III.

References

1. Pulte D, Brenner H (2010) Changes in survival in head and neck cancers in the late 20th and early 21st century: a period analysis. Oncologist 15(9):994–1001
2. Studer G, Linsenmeier C, Riesterer O et al (2013) Late term tolerance in head neck cancer patients irradiated in the IMRT era. Radiat Oncol 8:259
3. Huellner MW, Kuhn FP, Curtin HD (2015) FDG-PET/CT and FDG-PET/MR imaging in head and neck cancer. In: von Schulthess GK (ed) Molecular anatomic imaging: PET/CT, PET/MR and SPECT CT. Wolters Kluwer, Philadelphia, pp 341–361
4. Queiroz MA, Huellner MW (2015) PET/MR in cancers of the head and neck. Semin Nucl Med 45(3):248–265
5. Loeffelbein DJ, Souvatzoglou M, Wankerl V et al (2014) Diagnostic value of retrospective PET-MRI fusion in head-and-neck cancer. BMC Cancer 14:846
6. Loeffelbein DJ, Souvatzoglou M, Wankerl V et al (2012) PET-MRI fusion in head-and-neck oncology: current status and implications for hybrid PET/MRI. J Oral Maxillofac Surg Off J Am Assoc Oral Maxillofacial Surg 70(2):473–483
7. Queiroz MA, Hullner M, Kuhn F et al (2014) Use of diffusion-weighted imaging (DWI) in PET/MRI for head and neck cancer evaluation. Eur J Nucl Med Mol Imaging 41(12):2212–2221
8. Allal AS, Slosman DO, Kebdani T, Allaoua M, Lehmann W, Dulguerov P (2004) Prediction of outcome in head-and-neck cancer patients using the standardized uptake value of 2-[18F]fluoro-2-deoxy-D-glucose. Int J Radiat Oncol Biol Phys 59(5):1295–1300
9. Allal AS, Dulguerov P, Allaoua M et al (2002) Standardized uptake value of 2-[(18)F] fluoro-2-deoxy-D-glucose in predicting outcome in head and neck carcinomas treated by radiotherapy with or without chemotherapy. J Clin Oncol Off J Am Soc Clin Oncol 20(5):1398–1404
10. Goerres GW, Haenggeli CA, Allaoua M et al (2000) Direct comparison of F-18-FDG PET and ultrasound in the follow-up of patients with squamous cell cancer of the head and neck. Nuklearmedizin Nucl Med 39(8):246–250
11. Brun E, Kjellen E, Tennvall J et al (2002) FDG PET studies during treatment: prediction of therapy outcome in head and neck squamous cell carcinoma. Head Neck 24(2):127–135
12. Halfpenny W, Hain SF, Biassoni L, Maisey MN, Sherman JA, McGurk M (2002) FDG-PET. A possible prognostic factor in head and neck cancer. Br J Cancer 86(4):512–516
13. Minn H, Lapela M, Klemi PJ et al (1997) Prediction of survival with fluorine-18-fluoro-deoxyglucose and PET in head and neck cancer. J Nucl Med Off Publ Soc Nucl Med 38(12):1907–1911
14. Schwartz DL, Rajendran J, Yueh B et al (2004) FDG-PET prediction of head and neck squamous cell cancer outcomes. Arch Otolaryngol Head Neck Surg 130(12):1361–1367
15. Kuhn FP, Hullner M, Mader CE et al (2014) Contrast-enhanced PET/MR imaging versus contrast-enhanced PET/CT in head and neck cancer: how much MR information is needed? J Nucl Med Off Publ Soc Nucl Med 55(4):551–558
16. Gunzinger JM, Delso G, Boss A et al (2014) Metal artifact reduction in patients with dental implants using multispectral three-dimensional data acquisition for hybrid PET/MRI. EJNMMI Phys 1(1):102
17. Khafif A, Schneebaum S, Fliss DM et al (2006) Lymphoscintigraphy for sentinel node mapping using a hybrid single photon emission CT (SPECT)/CT system in oral cavity squamous cell carcinoma. Head Neck 28(10):874–879
18. Even-Sapir E, Lerman H, Lievshitz G et al (2003) Lymphoscintigraphy for sentinel node mapping using a hybrid SPECT/CT system. J Nucl Med Off Publ Soc Nucl Med 44(9):1413–1420
19. Haerle SK, Strobel K, Ahmad N, Soltermann A, Schmid DT, Stoeckli SJ (2011) Contrast-enhanced (1)(8)F-FDG-PET/CT for the assessment of necrotic lymph node metastases. Head Neck 33(3):324–329
20. Krogdahl AS (1979) Carcinoma occurring in branchial cleft cysts. Acta Otolaryngol 88(3–4):289–295
21. Kendi AT, Magliocca K, Corey A et al (2015) Do 18F-FDG PET/CT parameters in oropharyngeal and oral cavity squamous cell carcinomas indicate HPV status? Clin Nucl Med 40(3):e196–e200
22. Corey AS, Hudgins PA (2012) Radiographic imaging of human papillomavirus related carcinomas of the oropharynx. Head Neck Pathol 6(Suppl 1):S25–S40
23. Puri SK, Fan CY, Hanna E (2003) Significance of extracapsular lymph node metastases in patients with head and neck squamous cell carcinoma. Curr Opin Otolaryngol Head Neck Surg 11(2):119–123
24. Hirabayashi H, Koshii K, Uno K et al (1991) Extracapsular spread of squamous cell carcinoma in neck lymph nodes: prognostic factor of laryngeal cancer. Laryngoscope 101(5):502–506
25. Carter RL, Barr LC, O'Brien CJ, Soo KC, Shaw HJ (1985) Transcapsular spread of metastatic squamous cell carcinoma from cervical lymph nodes. Am J Surg 150(4):495–499
26. Johnson JT, Barnes EL, Myers EN, Schramm VL Jr, Borochovitz D, Sigler BA (1981) The extracapsular spread of tumors in cervical node metastasis. Arch Otolaryngol 107(12):725–729
27. Coatesworth AP, MacLennan K (2002) Squamous cell carcinoma of the upper aerodigestive tract: the prevalence of microscopic

extracapsular spread and soft tissue deposits in the clinically N0 neck. Head Neck 24(3):258–261
28. Stolzmann P, Veit-Haibach P, Chuck N et al (2013) Detection rate, location, and size of pulmonary nodules in trimodality PET/CT-MR: comparison of low-dose CT and Dixon-based MR imaging. Invest Radiol 48(5):241–246
29. Raad RA, Friedman KP, Heacock L, Ponzo F, Melsaether A, Chandarana H (2015) Outcome of small lung nodules missed on hybrid PET/MRI in patients with primary malignancy. J Magn Reson Imaging JMRI. doi:10.1002/jmri.25005
30. Chang ST, Nguyen DC, Raptis C et al (2015) Natural history of preoperative subcentimeter pulmonary nodules in patients with resectable pancreatic adenocarcinoma: a retrospective cohort study. Ann Surg 261(5):970–975
31. Edge SB, American Joint Committee on Cancer (2010) AJCC cancer staging manual, 7th edn. Springer, New York
32. Righi PD, Kelley DJ, Ernst R et al (1996) Evaluation of prevertebral muscle invasion by squamous cell carcinoma. Can computed tomography replace open neck exploration? Arch Otolaryngol Head Neck Surg 122(6):660–663
33. Loevner LA, Ott IL, Yousem DM et al (1998) Neoplastic fixation to the prevertebral compartment by squamous cell carcinoma of the head and neck. AJR Am J Roentgenol 170(5):1389–1394
34. Yousem DM, Hatabu H, Hurst RW et al (1995) Carotid artery invasion by head and neck masses: prediction with MR imaging. Radiology 195(3):715–720
35. Yu Q, Wang P, Shi H, Luo J (2003) Carotid artery and jugular vein invasion of oral-maxillofacial and neck malignant tumors: diagnostic value of computed tomography. Oral Surg Oral Med Oral Pathol Oral Radiol Endodont 96(3):368–372
36. Wagner M, Bjerkvig R, Wiig H et al (2012) Inflamed tumor-associated adipose tissue is a depot for macrophages that stimulate tumor growth and angiogenesis. Angiogenesis 15(3):481–495
37. Manzoor NF, Russell JO, Bricker A et al (2013) Impact of surgical resection on survival in patients with advanced head and neck cancer involving the carotid artery. JAMA Otolaryngol Head Neck Surg 139(11):1219–1225
38. Yousem DM, Gad K, Tufano RP (2006) Resectability issues with head and neck cancer. AJNR Am J Neuroradiol 27(10):2024–2036
39. Kuno H, Onaya H, Fujii S, Ojiri H, Otani K, Satake M (2014) Primary staging of laryngeal and hypopharyngeal cancer: CT, MR imaging and dual-energy CT. Eur J Radiol 83(1):e23–e35
40. Zbaren P, Caversaccio M, Thoeny HC, Nuyens M, Curschmann J, Stauffer E (2006) Radionecrosis or tumor recurrence after radiation of laryngeal and hypopharyngeal carcinomas. Otolaryngol Head Neck Surg Off J Am Acad Otolaryngol Head Neck Surg 135(6):838–843
41. Chu MM, Kositwattanarerk A, Lee DJ et al (2010) FDG PET with contrast-enhanced CT: a critical imaging tool for laryngeal carcinoma. Radiographics Rev Publ Radiol Soc North Am Inc 30(5):1353–1372
42. Loevner LA, Yousem DM, Montone KT, Weber R, Chalian AA, Weinstein GS (1997) Can radiologists accurately predict preepiglottic space invasion with MR imaging? AJR Am J Roentgenol 169(6):1681–1687
43. Paes FM, Singer AD, Checkver AN, Palmquist RA, De La Vega G, Sidani C (2013) Perineural spread in head and neck malignancies: clinical significance and evaluation with 18F-FDG PET/CT. Radiographics Rev Publ Radiol Soc North Am Inc 33(6):1717–1736
44. Curtin HD (2004) Detection of perineural spread: fat suppression versus no fat suppression. AJNR Am J Neuroradiol 25(1):1–3
45. Curtin HD (1998) Detection of perineural spread: fat is a friend. AJNR Am J Neuroradiol 19(8):1385–1386
46. Gandhi D, Gujar S, Mukherji SK (2004) Magnetic resonance imaging of perineural spread of head and neck malignancies. Top Magn Reson Imaging TMRI 15(2):79–85
47. Frunza A, Slavescu D, Lascar I (2014) Perineural invasion in head and neck cancers – a review. J Med Life 7(2):121–123
48. Moonis G, Cunnane MB, Emerick K, Curtin H (2012) Patterns of perineural tumor spread in head and neck cancer. Magn Reson Imaging Clin North Am 20(3):435–446
49. Abd El-Hafez YG, Chen CC, Ng SH et al (2011) Comparison of PET/CT and MRI for the detection of bone marrow invasion in patients with squamous cell carcinoma of the oral cavity. Oral Oncol 47(4):288–295
50. Delso G, Zeimpekis K, Carl M, Wiesinger F, Hullner M, Veit-Haibach P (2014) Cluster-based segmentation of dual-echo ultrashort echo time images for PET/MR bone localization. EJNMMI Phys 1(1):7
51. Delso G, Wiesinger F, Sacolick LI et al (2015) Clinical evaluation of zero-echo-time MR imaging for the segmentation of the skull. J Nucl Med Off Publ Soc Nucl Med 56(3):417–422
52. Wiesinger F, Sacolick LI, Menini A et al (2015) Zero TE MR bone imaging in the head. Magn Reson Med Off J Soc Magn Reson Med Soc Magn Reson Med. doi:10.1002/mrm.25545
53. Cabello J, Lukas M, Forster S, Pyka T, Nekolla SG, Ziegler SI (2015) MR-based attenuation correction using ultrashort-echo-time pulse sequences in dementia patients. J Nucl Med Off Publ Soc Nucl Med 56(3):423–429
54. Rasch C, Keus R, Pameijer FA et al (1997) The potential impact of CT-MRI matching on tumor volume delineation in advanced head and neck cancer. Int J Radiat Oncol Biol Phys 39(4):841–848
55. Sakata K, Hareyama M, Tamakawa M et al (1999) Prognostic factors of nasopharynx tumors investigated by MR imaging and the value of MR imaging in the newly published TNM staging. Int J Radiat Oncol Biol Phys 43(2):273–278
56. Mukherji SK, Wolf GT (2003) Evaluation of head and neck squamous cell carcinoma after treatment. AJNR Am J Neuroradiol 24(9):1743–1746
57. Som PM, Curtin HD, Mancuso AA (1999) An imaging-based classification for the cervical nodes designed as an adjunct to recent clinically based nodal classifications. Arch Otolaryngol Head Neck Surg 125(4):388–396
58. Trotta BM, Pease CS, Rasamny JJ, Raghavan P, Mukherjee S (2011) Oral cavity and oropharyngeal squamous cell cancer: key imaging findings for staging and treatment planning. Radiographics Rev Publ Radiol Soc North Am Inc 31(2):339–354